Adsorption of polycyclic aromatic hydrocarbons from wastewater by using silica-based organic–inorganic nanohybrid material

Ali Balati, Afsaneh Shahbazi, Mostafa M. Amini and Seyed Hossein Hashemi

ABSTRACT

Polycyclic aromatic hydrocarbons (PAHs) are a group of priority pollutants, which are classified as persistent hazardous contaminants. Herein, the adsorption of three PAHs, naphthalene (NAP), acenaphthylene (ACN), and phenanthrene (PHN), from wastewater onto NH_2-SBA-15 organic–inorganic nanohybrid material as a function of pH of the media (2–10), sorbent dosage (0.5–3.5 g L^{-1}), PAH concentration (1–18 mg g^{-1}), and temperature (25–45 °C) were elucidated. The prepared adsorbents were characterized by scanning electron microscope, transmission electron microscopy, X-ray diffractions, and thermogravimetric analysis. Among Langmuir, Freundlich, and Temkin isotherms models, it was found that the Langmuir model gave an excellent overall fit ($R^2 > 0.97$). The maximum adsorption capacity of 1.92, 1.41, and 0.76 mg g^{-1} was obtained for NAP, ACN, and PHN, respectively. Adsorption kinetics of PAHs onto NH_2-SBA-15 was in accordance with the pseudo-second-order model, providing evidence that pore mass transferring was involved. PAHs' adsorption was strongly dependent on temperature, and confirmed the spontaneous and endothermic nature of the process. The optimized sorption condition was successfully applied to the real petroleum refinery wastewater samples and the adsorption capacity of NH_2-SBA-15 was satisfactory for PAHs' studies as 1.67, 1.06, and 0.24 mg g^{-1} for NAP, ACN and PHN, respectively. Furthermore, reusability was successfully tested by five sequential recoveries.

Key words | adsorption modeling, NH_2-SBA-15, PAHs, petroleum refinery, real wastewater

Ali Balati
Afsaneh Shahbazi (corresponding author)
Seyed Hossein Hashemi
Environmental Sciences Research Institute,
Shahid Beheshti University,
G.C.,
Tehran 1983963113,
Iran
E-mail: *a_shahbazi@sbu.ac.ir*

Mostafa M. Amini
Department of Chemistry,
Shahid Beheshti University,
G.C.,
Tehran 1983963113,
Iran

INTRODUCTION

Polycyclic aromatic hydrocarbons (PAHs) are a class of diverse organic compounds that are included in the European Union and United States Environmental Protection Agency priority pollutant list due to their mutagenic, carcinogenic, and endocrine-disrupting properties. They are ubiquitous environmental contaminants and have been shown to accumulate in coastal estuarine and marine sediments as well as aquatic organisms (Khalili-Fard *et al.* 2012). Anthropogenic sources of PAHs in the environment originate from coal and oil combustion, waste incineration, coal gasification and liquefaction processes, production of coke, carbon black, coal tar pitch, asphalt, and wastewater from petrochemical plants (Prabhukumar & Pagilla 2010). PAHs are often resistant to biological degradation and are not efficiently removed by conventional physicochemical methods such as coagulation, flocculation, sedimentation, filtration, or ozonation (Crisafully *et al.* 2008). Among different types of remediation technologies, adsorption is one of the simplest, most effective, quick, and widely applicable techniques. Using adsorption is applicable for various pollutants such as organic compounds and heavy metals by selecting the type of adsorbent and adsorption conditions (Sasaki & Tanaka 2011). Various types of sorbents have been proposed for the removal of PAHs, for example,

doi: 10.2166/wrd.2014.013

activated carbon (Augulyte *et al.* 2009), zeolites (Lemić *et al.* 2007), carbon nanoporous (Anbia & Moradi 2009), hydrophobic magnetite (Tang *et al.* 2013), organobentonite (Wu & Zhu 2012), and silica-based mesoporous materials (SBMM) (Vidal *et al.* 2011). The SBMM were good candidates for the adsorptive removal of organic pollutants from aqueous solution due to their high surface area, large and uniform pore size, thermal and mechanical stability, tunable pore structure, as well as extraordinarily wide possibilities of functionalization (Shahbazi *et al.* 2012). It has been reported that SBMM can be used as potential adsorbents for various organic pollutants such as lysine, nitrobenzene, pharmaceuticals, and dyes (Chen *et al.* 2012). Despite the increase in application of SBMM in wastewater treatment studies, very limited studies have been carried out regarding the removal of PAHs from synthetic, and especially, real wastewaters. Among SBMM, SBA-15 with (two-dimensional) 2D hexagonal arrangements, highly ordered pore distribution and large pore volume, has been approved as an efficient adsorbent for various large organic pollutants (Kosuge *et al.* 2007). Also, it is possible to alter its surface chemistry by grafting with suitable functional groups (Bui *et al.* 2011). In this context, the development of functionalized SBA-15 for PAHs' adsorption has generated a considerable amount of interest (Hu *et al.* 2009).

It is well-known that a weak interaction can be established between a rich and a poor electron π system (Wei *et al.* 2008). Such interactions usually result in the formation of a charge transfer complex and can be used in a process for adsorption of aromatic pollutants (Sevignon *et al.* 2005). In this context, in the present study NH_2 group was grafted onto SBA-15 mesoporous silica with the aim of evaluating the feasibility of NH_2-SBA-15 organic–inorganic nanohybrid material in the elimination of three relevant PAHs (naphthalene (NAP), acenaphthylene (ACN), and phenanthrene (PHN)) from synthetic and real petroleum wastewater in a batch technique. The effects of adsorbent dose, solution pH, PAH concentration, contact time, and temperature were investigated. Entire studies of equilibrium, kinetics, and thermodynamics were also conducted to provide a depth of understanding of the adsorption features of three selected PAHs onto NH_2-SBA-15 organic–inorganic nanohybrid.

MATERIALS AND METHODS

Chemicals and reagents

Tetraethyl orthosilicate (TEOS, 98%), 3-aminopropyltrimethoxysilane (APS, 98%), dry toluene (99.9%), HCl (37%), methanol, NAP, ACN, and PHN were purchased from Merck. Pluronic P123 ($Mw = 5{,}800\ g\ mol^{-1}$; EO_{20}–$PO_{70}EO_{20}$) was purchased from Aldrich. All aqueous solutions were prepared using double distilled water. The physicochemical properties of the three studied PAHs are presented in Table 1. It can be seen that these substances have low solubility in water, which tended to be even lower when the number of aromatic rings was increased. Hence, in PAH adsorption experiments, there are two vulnerabilities, incomplete dissolution of PAHs in water and loss of PAHs by volatilization, especially during centrifuge. To overcome these conflicts, PAHs were dissolved in methanol/water solution. In this case, tests were performed on blanks (various methanol/water ratios in the presence of PAHs without adding adsorbent for testing evaporation) to

Table 1 | Physicochemical properties of studied PAHs

PAHs	Structure	Molecular weight ($g\ mol^{-1}$)	Vapour pressure at 25 °C Pa	Water solubility ($g\ L^{-1}$)	log K_{ow}
Naphthalene $C_{10}H_8$		128	10.4	31 ~	3.37
Acenaphthylene $C_{12}H_8$		152	9.0×10^{-1}	3.9	4.00
Phenanthrene $C_{14}H_{10}$	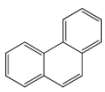	178	2.0×10^{-2}	1.2	4.57

quantify an appropriate methanol/water ratio. For testing the effect of methanol on PAHs' adsorption, batch adsorption experiments were carried out at various methanol/water ratios. In this case, any changes in PAHs' removal were not observed by increasing methanol/water ratios up to 20% v/v. Therefore, at the level of 20% we found an appropriate condition in which methanol had no measurable effect on adsorption and PAH losses by evaporation were minimized. Thus, the solutions used in the adsorption experiments were prepared immediately prior to use, by diluting the stock solution and adjusting the methanol concentration to 20% v/v.

Synthesis of NH_2-SBA-15

The SBA-15 silica was synthesized according to an earlier report (Zhao *et al.* 1998b). In a typical synthesis, 4.0 g of P123 was dispersed in 120 g of water and 8.64 g of 2 M HCl solution at 40 °C while stirring, and this was followed by addition of 8.54 g of TEOS to obtain the homogenous solution. This gel mixture was continuously stirred at 40 °C for 24 h and finally crystallized in a Teflon-lined autoclave at 100 °C for 2 days. After cooling, the solid product was filtered, and template removal was achieved by calcination in air at 600 °C for 6 h and SBA-15 silica was obtained. The prepared SBA-15 (1.0 g) was suspended in 30 mL of dry toluene, and 4 mL of APS was added under a dry nitrogen atmosphere and then the mixture was refluxed for 10 h. The solid product was recovered by filtration, washed with dichloromethane and ethanol, and dried in air. Finally, material was extracted with a Soxhlet extractor with a mixture of ethanol and dichloromethane (1:1), in order to remove the silylating reagent residue, and dried at 70 °C under a vacuum overnight (Shahbazi *et al.* 2011).

Characterization

The X-ray diffractions (XRD) were recorded on a Philips 1830 powder X-ray diffractometer, using the Cu-Kα radiation over a range of 0.8° to 6.0°, with a 2θ step size of 0.01° and a step time of 1 s. The morphology of the SBA-15 was observed by scanning electron microscope (SEM, LEO 1455VP, Cambridge, UK). The transmission electron microscopy (TEM) images were taken on a JEOL JEM-2100F field emission transmission electron microscope at an acceleration voltage of 200 kV. Fourier transform infrared (FTIR) spectra of prepared materials were recorded (KBr pellets) on a Shimadzu model FTIR 4600 spectrometer in the range of 400–4,000 cm^{-1}. Thermogravimetric analysis (TGA/DTA) was carried out on a Rheumatic Scientific STA-503 with a heating rate of 10 °C/min in air from an ambient temperature up to 750 °C. Single point BET (Brunauer–Emmett–Teller) surface area was measured by nitrogen adsorption technique using a Micromeritics ASAP 2010 analyzer.

Batch adsorption experiments

Adsorption experiments were conducted in glass Erlenmeyer flasks (25 mL) sealed with PVC film and a magnetic stirrer device set to operate at 150 rpm and 25 ± 1 °C. Due to the relatively low water solubility of PAHs generally, stock solutions were initially prepared in pure methanol. Typically, the concentration of methanol in the synthetic wastewater was maintained at not more than about 20 vol%. There was no considerable adsorption of analytes on the walls of the flasks in the adsorption experiments, which was verified by comparing the PAH concentrations in reaction mixtures with and without the adsorbent (blank). The influences of experimental parameters such as pH (2–10, step size: 1), adsorbent dosage (0.5–3.5, g L^{-1}), and PAH concentration (1–18 mg L^{-1}) were studied. The pH of solutions was adjusted by adding negligible volumes (0–15 μL) of 0.1 M HCl or 0.1 M NaOH. The equilibrium adsorption study was primarily carried out by sampling at regular intervals of time to optimize the contact time of the adsorption process. It could be seen that the adsorbed amount of PAH increased with contact time up to 24 h, after which maximum removal is attained. Therefore, the equilibrium time of 24 h was selected as the optimum contact time for all further experiments. After equilibrium, the adsorbent was removed by centrifugation at 10,000 rpm for 10 min (centrifuge HERMLE Z 323 K), and the respective solution analyzed by a UV-Vis spectrophotometer (UV-Vis 2100 Shimadzu) for NAP, ACN, and PHN at λ_{max} of 220.5, 225.4, and 250.0 nm, respectively. Daily calibration curves before each set of measurements were drawn. The removal efficiency ($R\%$) and the adsorption capacity (q_e) of the

NH_2-SBA-15 were calculated using Equations (1) and (2), respectively

$$R = \frac{C_0 - C_t}{C_o} \times 100 \quad (1)$$

$$q_e = \frac{(C_0 - C_e)V}{W} \quad (2)$$

where $R\%$ is the removal efficiency of the PAHs and q_e adsorption capacity, C_0 the initial concentration, C_e the equilibrium (final) concentration, and C_t the concentration of the PAHs at t time (mg L^{-1}). V is the volume of the solution (mL) and W the mass of the adsorbent (g).

Adsorption modeling

The adsorption feature was completely studied by isotherm, kinetic, and thermodynamic modeling of sorption experimental data of three studied PAHs (NAP, ACN, and PHN) onto NH_2-SBA-15. Adsorption isotherm experiments were conducted by adding 0.06 g of NH_2-SBA-15 to 20 mL of the PAH solution (20% v/v methanol) at 25 °C and pH 5 by predetermined concentrations (1–18 mg L^{-1}) of NAP, ACN, and PHN. The adsorption isotherm data were fitted by the three isotherm models of Langmuir, Freundlich, and Temkin.

The Langmuir isotherm assumes a surface with homogeneous binding sites, equivalent sorption energies, and no interaction between adsorbed species (Lombardo *et al.* 2012). Its mathematical form is written as:

$$q_e = \frac{q_m b C_e}{1 + bC_e} \quad (3)$$

The favor ability adsorption was checked by using a dimensionless separation parameter R_L, according to the following equation:

$$R_L = \frac{1}{1 + bC_0} \quad (4)$$

where q_m and b represent the maximum adsorption capacity (mg g^{-1}) and the energy constant (L g^{-1}) related to the heat of adsorption, respectively. The value of R_L indicates the type of the isotherm to be either unfavorable ($R_L > 1$), linear ($R_L = 1$), favorable ($0 < R_L < 1$), or irreversible ($R_L = 0$) (Shahbazi *et al.* 2011).

The Freundlich isotherm is an empirical equation based on an exponential distribution of adsorption sites and energies (Shahbazi *et al.* 2011). It is represented as

$$q_e = K_f C_e^{1/n} \quad (5)$$

where K_f (mg$^{(n-1)/n}$ g^{-1} L^{-1}) and n are Freundlich adsorption isotherm constants, indicative of the saturation capacity and intensity of adsorption, respectively. It is well-known that $1/n$ value between 0.1 and 1 indicates a favorable adsorption (Vidal *et al.* 2011).

The Temkin isotherm assumes that decrease in the heat of adsorption is linear and the adsorption is characterized by a uniform distribution of binding energies. The Temkin isotherm is expressed by the following equation (Temkin & Pyzhev 1940):

$$q_e = q_m + \ln(aC_e) \quad (6)$$

where q_m (mg g^{-1}) is the maximum adsorption capacity, and constant a (mol^{-1}) corresponds to the maximum binding energy.

Adsorption kinetic experiments were carried out by adding 0.06 g of NH_2-SBA-15 into 20 mL of solution (20% v/v methanol) containing each PAH (6 mg L^{-1} of NAP and ACN, and 4 mg L^{-1} of PHN) and stirred continuously at 25 °C and pH 5. Adsorption experiments were conducted at various periods of time (0.25–72 hours). Three adsorptions kinetic models were established to understand the adsorption kinetics nature, namely pseudo-first-order (Equation (7)), pseudo-second-order (Equation (8)), and Weber–Morris intra-particle diffusion (Equation (9)) kinetic models (Hamoudi & Belkacemi 2013)

$$\log(q_e - q_t) = \log q_e - \frac{k_1}{2.303} t \quad (7)$$

$$\frac{t}{q_t} = \frac{1}{k_2 q_e^2} + \frac{t}{q_e} \quad (8)$$

$$q_t = k_f \times t^{0.5} + B \quad (9)$$

where q_e and q_t are the amounts of PAHs adsorbed (mg g^{-1}) at equilibrium at time t (hour), respectively, k_1 (h^{-1}) and k_2 (g mg^{-1} h^{-1}) are rate constant of pseudo-first-order and pseudo-second-order kinetic models, respectively. The k_f is the intraparticle diffusion rate constant (mg g^{-1} $h^{-0.5}$) and B (mg g^{-1}) a constant that gave an idea about the thickness of the boundary layer in the Weber–Morris constant.

All the nonlinear regression analysis was carried out with SigmaPlot software (SigmaPlot 12.0, SPSS Inc., USA) in order to predict isotherm parameters.

In addition, the adsorption experiments were carried out at different temperatures (25, 35, and 45 °C) to evaluate thermodynamic criteria. Qualitative estimation of the thermodynamic properties of the adsorption process, such as enthalpy change (ΔH, kJ mol^{-1}), entropy change (ΔS, J^{-1} mol^{-1} K^{-1}), and Gibbs free energy change (ΔG, J mol^{-1}), were calculated using Equations (10) to (12) (Shahbazi *et al.* 2011)

$$ln\ K_d = \frac{\Delta S}{R} - \frac{\Delta H}{RT} \tag{10}$$

$$K_d = \frac{C_0 - C_e}{C_e} \times \frac{V}{W} \tag{11}$$

$$\Delta G = \Delta H - T\,\Delta S \tag{12}$$

where the values of ΔH and ΔS were obtained from the slope and intercept of ln k_d vs. $1/T$ plots, respectively. T is the temperature in K and R the universal gas constant (8.314 J mol^{-1} K^{-1}). The sorption distribution coefficient (k_d, L g^{-1}) was calculated by division of q_e to C_e. The V is the working volume in L and W the adsorbent mass in g.

Recovery experiments

To make the sorbent economically competitive, the prepared NH_2-SBA-15 sorbent should be reused 'n' number of adsorption–desorption cycles (Shahbazi *et al.* 2011). First, the sorption process was preceded by adding 0.06 mg of adsorbent into 20 mL of each PAH solution (NAP, ACN, and PHN with a concentration of 6, 6, and 4 mg L^{-1}, respectively). The mixture was stirred at 25 °C and pH 5 for 24 hours. After that, in order to recover PAHs from NH_2-SBA-15, the sorbent was completely separated from the liquid phase and transferred into 50 mL of methanol and stirred for 4 hours. In each step, the concentration of each studied PAH was measured in liquid phase. The cycles of adsorption–desorption processes were successively conducted five times. The PAH recovery was calculated by the following equation:

$$\text{PAH recovery} = \frac{\text{Amount of PAH desorbed}}{\text{Amount of PAH adsorbed}} \times 100 \tag{13}$$

RESULTS AND DISCUSSION

Characterization of adsorbent

The low-angle XRD pattern of SBA-15 and NH_2-SBA-15 are shown in Figure 1(a). The two synthesized adsorbents

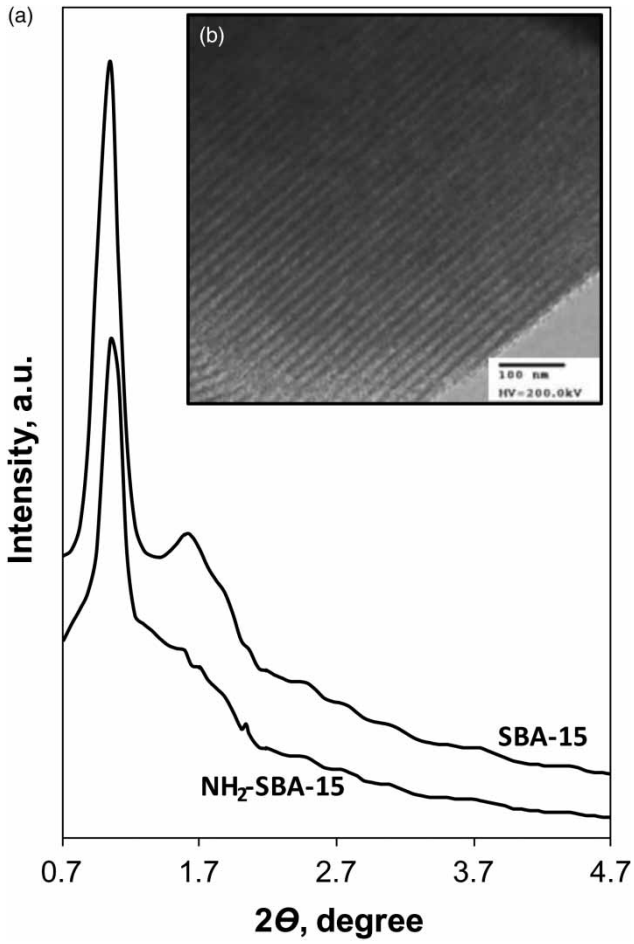

Figure 1 | (a) XRD patterns of SBA-15 and NH_2-SBA-15 and (b) TEM image of SBA-15.

exhibited a single strong peak (1 0 0) followed by two additional peaks (1 1 0, 2 0 0) which could be associated with two-dimensional hexagonal *P*6 mm symmetry, indicating a well-defined SBA-15 mesostructure (Aguado *et al.* 2009). The intensity of the XRD peak for NH_2-SBA-15 was substantially lower than that measured for SBA-15, which associated with the pore filling effect of the SBA-15 channels or the anchoring ligands on the outer surface of SBA-15 (Asouhidou *et al.* 2009; Shahbazi *et al.* 2012). The TEM image of SBA-15 (Figure 1(b)) shows well-ordered hexagonal arrays of mesoporous (1D channel) and further confirmed that SBA-15 has a 2D *p*6 mm hexagonal structure. Channel direction of the 2D-hexagonal structures is parallel to the thickness direction of the nanostructured hexagonal platelet morphologies. The SEM micrograph (Figure 2) revealed that the SBA-15 consists of many rope-like domains with a relatively uniform length of 1 μm. The obtained morphology is in good agreement with the SBA-15 morphology presented in previous reports (Zhao *et al.* 1998a; Aguado *et al.* 2009; Shahbazi *et al.* 2011). The incorporation of amine groups in the silicate frameworks is confirmed by FTIR (Figure 3). The bands around 810 and 1,088 cm^{-1} signified the typical symmetric and asymmetric stretching of Si–O–Si, respectively (Bereket *et al.* 1997). The broad peak around 3,433 cm^{-1} is due to the O–H stretching vibration of the adsorbed water. The band at about 1,576 cm^{-1} is attributed to NH_2 bending, in the NH_2-SBA-15 sample, indicating the presence of primary amine (Bereket *et al.* 1997; Shahbazi *et al.* 2011). The stretching bands at 2,870 and 2,938 cm^{-1} are attributed to asymmetric and symmetric C–H stretching in the propyl chain (NH_2-SBA-15 spectrum).

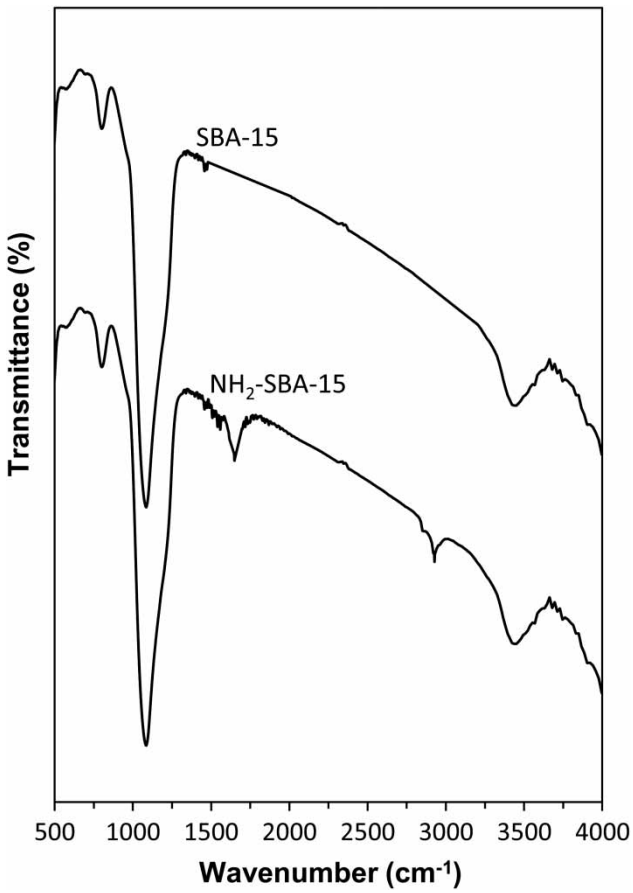

Figure 3 | FTIR spectra of SBA-15 and NH_2-SBA-15.

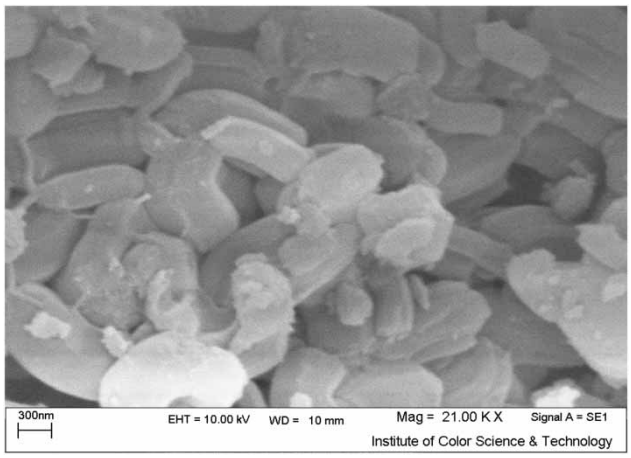

Figure 2 | SEM image of SBA-15.

TGA/DTA analysis of SBA-15 and NH_2-SBA-15 is shown in Figures 4(a) and 4(b), respectively. The weight loss around 175 °C in the TGA curve of bare SBA-15 is attributed to the dehydroxylation of the silicate network, which is endowed with hydroxyl groups before reaction with APS and formation of organic–inorganic nanohybrid material. Interestingly, after functionalization of SBA-15 the entire thermal analysis pattern is changed. The weight loss observed below 150 °C in the TGA curve of NH_2-SBA-15 is associated with desorption of the physically adsorbed water and between 300 and 650 °C to combustion of the organic moieties. The aminopropyl loaded on the surface of SBA-15 was calculated to be about 1.80 mmol g^{-1}. Single point BET analysis showed a surface area of 690 and 560 m^2 g^{-1} for SBA-15 and NH_2-SBA-15, respectively. Decreasing of surface in NH_2-SBA-15 corresponds to

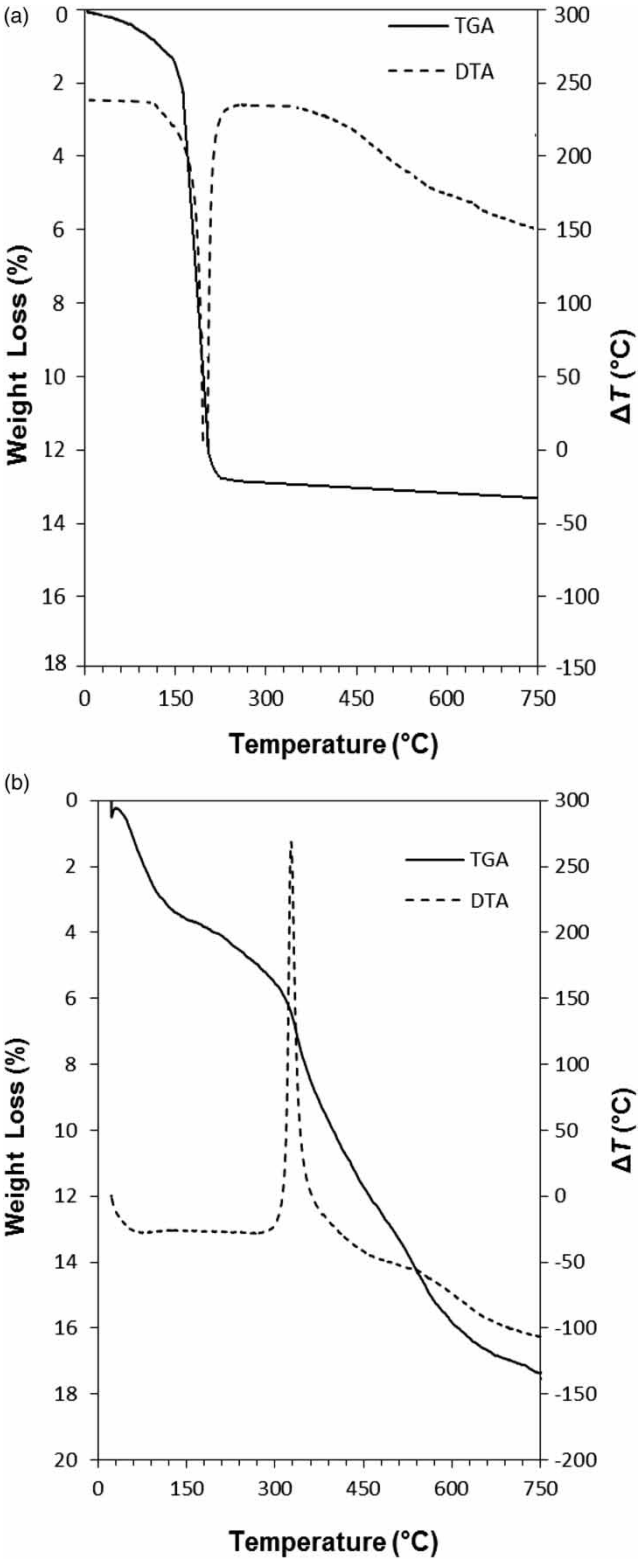

Figure 4 | TGA/DTA curves of (a) SBA-15 and (b) NH_2-SBA-15.

functionalization of the SBA-15 surface by APS (Shahbazi *et al.* 2011, 2012).

Effect of adsorbent dosage and pH

Due to the almost same physico-chemical properties of NAP and two other adsorbate materials (ACN and PHN), NAP was chosen as a representative sample to study PAHs for the investigation of the effect of pH and adsorbent dosage on sorbent efficiency. The removal of NAP as a function of NH_2-SBA-15 dosage is shown in Figure 5(a). As can be seen, the removal efficiency of NAP increased significantly as the adsorbent dosage was increased from 0.5 to 3.5 g L^{-1}. The percentage adsorption increased from 29.9 at the lower adsorbent dose (0.5 g L^{-1}) to 53.6 at the higher adsorbent dose (3.5 g L^{-1}) due to the increase in contact surface of adsorbent and the greater availability of the adsorbent (Namasivayam & Kavitha 2002). In the range of 0.5–1.0 g L^{-1} of NH_2-SBA-15, NAP adsorption increased almost linearly with adsorbent dosage and removal percentage reached 40.1%. Approximately near 3.0 g L^{-1} of NH_2-SBA-15 adsorbent dosage, the percentage of naphthalene removal almost stabilized. Hence, the optimum dosage was taken as 3.0 g L^{-1} for further studies.

The pH of the solution affected the surface charge of the adsorbents as well as the degree of ionization and speciation of different pollutants. This subsequently led to a shift in reaction kinetic and equilibrium characteristics of the sorption process (Srivastava *et al.* 2006). The removal efficiency of NAP onto NH_2-SBA-15 at various pH (2–10) is presented in Figure 5(b). As pH decreased from 8 to 2, the removal percentage increased and maximum removal percentage (79.3%) occurred at pH 2. In the pH range of 8–10, the removal percentage of NAP was obtained (50.8–62.3%). The reason for the higher removal rate at lower pH can be attributed to the formation of NH_3^+ on the surface of NH_2-SBA-15 and, consequently, increase of electrostatic interaction between surface charges of adsorbent and PAH's charge due to the π-electron-rich character of PHA compounds. However, the maximum PAH removal was achieved at pH 2, but the pH 5 was chosen for further studies because this pH was much closer to real wastewater that pH 2.

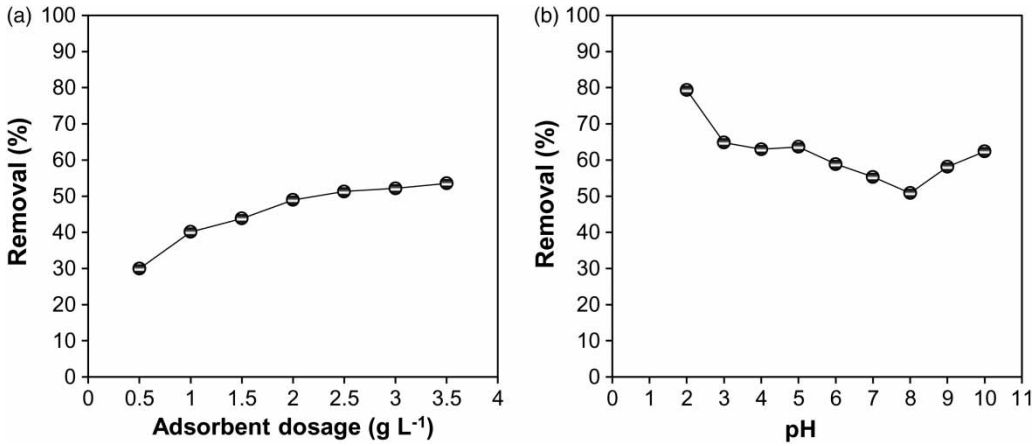

Figure 5 | (a) Effect of adsorbent dose at pH 5 and (b) effect of pH changes at adsorbent dosage of 3 g L^{-1} on removal percentage of NAP (conditions: NAP concentration 7 mg L^{-1}, temperature 25 °C).

Adsorption isotherms

Study of the adsorption equilibrium isotherms is an important step in investigating adsorption processes, since it can possibly identify the relationship between the amounts of analyte adsorbed and in solution, after equilibrium is reached (Vidal *et al.* 2011). Adsorption of NAP, ACN, and PHN onto NH_2-SBA-15 were modeled using the Freundlich, Langmuir, and Temkin isotherms (Figure 6). The fitness of models was assessed using the correlation coefficient (R^2) along with the lowest difference between experimental and predicted maximum sorption capacity (q_{max}). The parameters of the models are summarized in Table 2. The experimental maximum adsorption capacities of the three adsorbates followed an order of NAP (1.63 mg g^{-1}) > ACN (1.01 mg g^{-1}) > PHN (0.60 mg g^{-1}). All isotherms studies showed a sharp initial slope indicating high efficiency of the NH_2-SBA-15 for removal of PAHs at low concentrations due to a great number of adsorption sites available to surrounding PAH molecules. At high concentrations, adsorption sites became saturated and the isotherm reached a plateau. Among isotherm studies, the Langmuir model showed the best fit to data according to the highest R^2 and also there is good agreement between calculated Langmuir isotherm constant ($q_{max,\ cal}$) of NAP, ACN, and PHN and experimental results ($q_{e,\ exp}$) (Table 2). To clarify the favorableness of adsorption of each PAH, the separation factor (R_L) was also calculated, and results are summarized in Table 2. The evaluated values of R_L in the range of 0.1–0.7 indicate the Langmuir isotherm is favorable for modeling the data. According to the Freundlich constant (Table 2), the values of n were greater than unity (>2.9) indicating adsorption favorability. In this case, the sorption isotherm followed the L-type isotherm illustrating a high affinity between adsorbate and adsorbent (Jiang *et al.* 2002). The Temkin equation provided less agreement with experimental data (Figure 6), which could confirm the earlier hypothesis that the adsorption process was not controlled by chemical adsorption.

For comparing the adsorption capacity of NH_2-SBA-15 with that of unfunctionalized SBA-15, the absorption experiment was conducted in the same conditions (initial PAH concentration of 18 mg L^{-1}, pH 5, dosage of 3 g L^{-1}, and temperature of 25 °C). According to the results, in the case of NH_2-SBA-15 the adsorption capacity is around 2–4 times higher than for unfunctionalized SBA-15 (0.6–1.7 mg g^{-1} vs. 0.1–0.85 mg g^{-1}). Therefore, adsorption capacity could be enhanced by amine groups.

Adsorption kinetics

The adsorption phenomenon is a manifestation of complicated interactions among adsorbent, adsorbate, and solvent involved. The affinity between the adsorbent and the adsorbate was the main factor controlling the adsorption process (Pérez-Gregorio *et al.* 2010). The adsorption kinetic of NAP, ACN, and PHN onto NH_2-SBA-15 is shown in Figure 7. To evaluate the kinetic of the adsorption process,

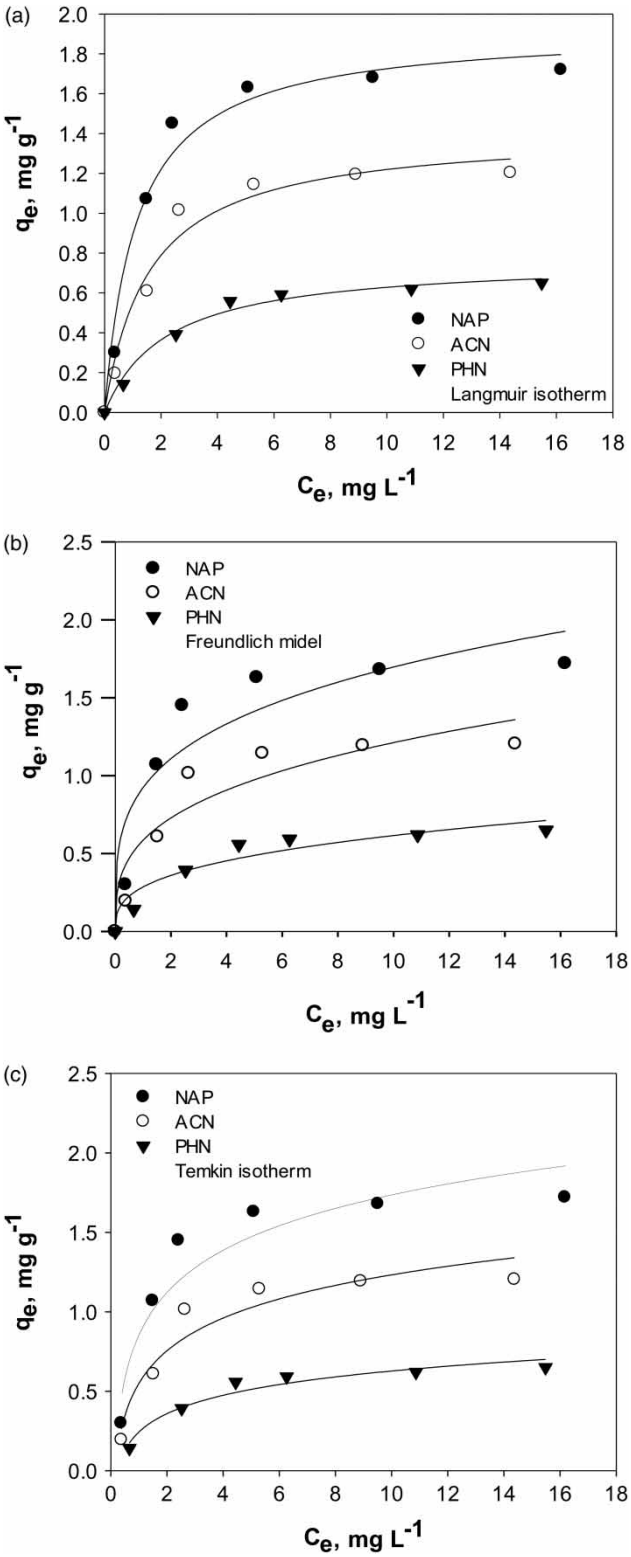

Figure 6 | Langmuir, Freundlich, and Temkin isotherms for NAP, ACN, and PHN adsorption onto NH_2-SBA-15 (conditions: pH 5, dosage 3 g L^{-1}, temperature 25 °C).

the data were modeled by the pseudo-first-order, pseudo-second-order, and Weber–Morris (Figures 7 and 8). According to Figure 7 and Table 3, the adsorption of the three studied PAHs followed the pseudo-second-order kinetic model due to its high correlation coefficients compared to pseudo-first-order model. Furthermore, the pseudo-second-order kinetic model indicated a fairly good agreement between the experimental adsorption capacity ($q_{e,\ exp}$) and the calculated adsorption capacity ($q_{e,\ cal}$) for the three studied PAHs. The pseudo-second-order kinetic model provided data to describe adequately both fast and slow adsorption steps. Several investigations reported that the pseudo-second-order kinetic model represented good experimental adsorption data for PAH adsorption using a variety of adsorbents, such as zeolite (Chang *et al.* 2004), activated carbon (Cabal *et al.* 2009), and organo-sepiolite (Gök *et al.* 2008).

According to the Weber–Morris model (plot of q_t versus $t^{0.5}$) the multi-linearity of this plot (Figure 8) for adsorption of NAP, ACN, and PHN onto NH_2-SBA-15 confirmed that the sorption occurred in three phases: (i) boundary layer and film diffusion, followed by (ii) intraparticle diffusion in the inner porosity of the SBMM, and finally (iii) the equilibrium. The initial steeper linear steps indicated that the surface or film diffusion processes had occurred. The second linear step corresponded to gradual sorption step where moving the PAH molecules into the interior nanoporous structure of NH_2-SBA-15 and pore diffusion was rate-limiting. The final step was due to reach equilibrium condition (Ofomaja 2010). It was also suggested that the intraparticle diffusion was not the only rate-limiting step because the plot did not pass through the origin. Similar behavior has been reported for various aromatic adsorbates onto porous adsorbents (Hall *et al.* 2009). The intraparticle diffusion rate constant k_i was calculated from the slope of the second linear step and is summarized in Table 3. The values of k_i obtained were 0.15, 0.12, and 0.06 for NAP, CAN, and PHN, respectively. The intercept of the plot provides an estimation of the thickness of the boundary layer, i.e., the larger the intercept value the greater is the boundary layer effect (Oubagaranadin *et al.* 2007). The diffusion rate parameters (k_i) indicated that the intraparticle diffusion controlled the sorption rate, which was the slowest step of the sorption process. In this step of sorption, the value of

Table 2 | Isotherm parameters of NAP, ACN, and PHN adsorption onto NH_2-SBA-15

		PAHs		
Isotherm models	**Parameters**	**NAP**	**ACN**	**PHN**
Langmuir	$q_{m,\exp}$ (mg g^{-1})	1.63	1.01	0.60
	$q_{m,\mathrm{cal}}$ (mg g^{-1})	1.92	1.41	0.76
	b(L g^{-1})	0.864	0.630	0.451
	R^2	0.979	0.976	0.989
	R_L	0.1–0.5	0.1–0.3	0.1–0.7
Freundlich	K_F ($mg^{(n-1)/n}$ g^{-1} L^{-1}	0.922	0.584	0.284
	$1/n$	0.265	0.316	0.334
	R^2	0.881	0.901	0.924
Temkin	q_m (L g^{-1})	9.94	6.35	4.29
	a (J mol^{-1})	5997.7	7651.3	13614.1
	R^2	0.943	0.957	0.972

intercept (B, mg g^{-1}) follows an order of ACN (0.67) >NAP (0.61) >PHN (0.11). Larger intercept suggests that surface diffusion had a larger role as the rate-limiting step. Hence, the increasing of intercept with the increasing of molecule weight suggested that the surface diffusion became more important for larger PAHs.

Adsorption thermodynamics

Understanding the thermodynamics of the adsorption is critical for the development of more efficient adsorbents suitable for real wastewater applications. The thermodynamic parameters of ΔH and ΔS were calculated from the slope and intercept plots of $\ln(K_L)$ vs. $1/T$, respectively (Figure 9), and ΔG was calculated from Equation (12). The thermodynamic parameters and correlation coefficients are summarized in Table 4.

Negative values of ΔG indicated spontaneous PAH adsorption and the degree of spontaneity of the adsorption increased with increasing temperature (Table 4). The values of ΔG smaller than 8 kJ mol^{-1} are characteristic of a physisorption mechanism while values between 8 and 16 kJ mol^{-1} indicate a chemisorption mechanism (Balan *et al.* 2009). For all three PAHs studied, values of ΔG were less than 8 kJ mol^{-1}, suggesting the process involved was physisorption. The positive enthalpy changes indicated that adsorption of NAP, ACN, and PHN onto NH_2-SBA-15 was endothermic. This is in agreement with the adsorption of organic pollutants with different adsorbents (Zhao *et al.* 2011; Sherif *et al.* 2012; Yang *et al.* 2013). The enthalpy value for a sorption process may be used to distinguish between chemical and physical sorption. For chemical sorption, values of enthalpy changes range from 83 to 830 kJ mol^{-1}, while for physisorption they range from 8 to 25 kJ mol^{-1} (Vijayakumar *et al.* 2012). The low values of ΔH (19.6–43.2 kJ mol^{-1}) provided evidence that the interaction between adsorbate and adsorbent is weak. On this basis, it was concluded that PAHs physically adsorbed onto NH_2-SBA-15. The positive entropy changes indicated that the degree of freedom increased at the solid–liquid interface during the adsorption of the studied PAHs on NH_2-SBA-15 organic–inorganic nanohybrid. In fact, the PAH molecules in solution were surrounded by a tightly bound hydration layer where water/methanol (20% v/v) molecules were more highly ordered than in the bulk water. When a molecule of PAHs was close to the hydration surface of NH_2-SBA-15 organic–inorganic nanohybrid, the ordered water molecules in these two hydration layers are compelled and disturbed, thus increasing of entropy proceeded. Although the adsorption of PAH molecules on NH_2-SBA-15 decreased the degree of freedom of PAH molecules, it seems likely that positive entropy associated with the adsorption of PAHs on NH_2-SBA-15 may be due to the increase in entropy of water molecules in the aquatic media.

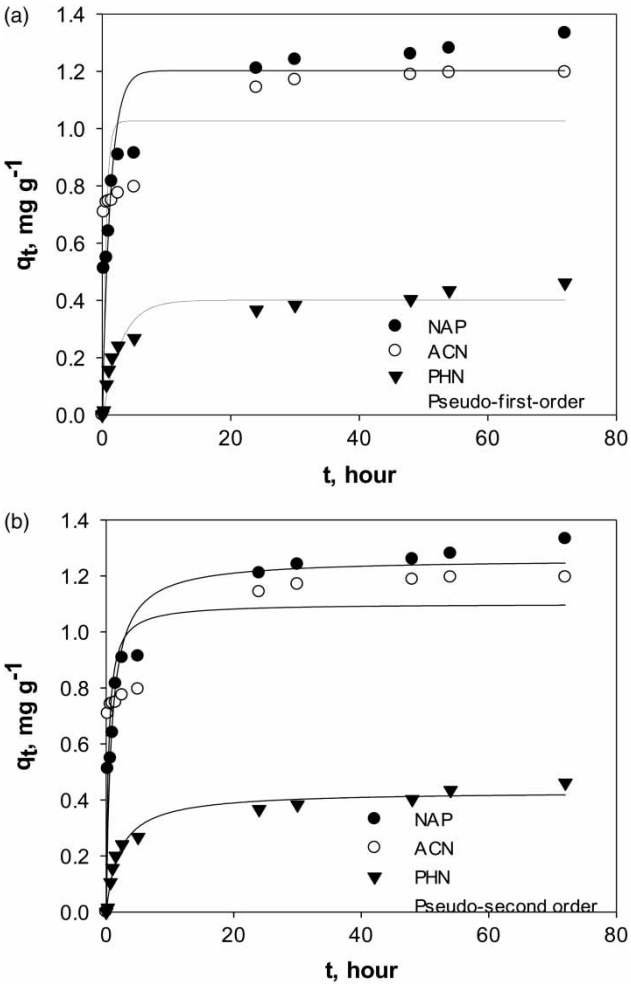

Figure 7 | Pseudo-first-order and pseudo-second-order kinetics for NAP, ACN, and PHN adsorption onto NH_2-SBA-15 (conditions: pH 5, dosage 3 g L^{-1}, initial concentration of NAP, ACN, and PHN of 6, 6, and 4 mg L^{-1}, respectively).

Table 3 | Kinetic parameters of NAP, ACN, and PHN adsorption onto NH_2-SBA-15

		PAHs		
Kinetic models	**Parameters**	**NAP**	**ACN**	**PHN**
Pseudo-first-order	$q_{e,\ exp}$ (mg g^{-1})	1.66	1.19	0.46
	$q_{e,\ cal}$ (mg g^{-1})	1.20	1.02	0.403
	k_1 (h^{-1})	0.78	2.06	0.361
	R^2	0.942	0.837	0.975
Pseudo-second-order	$q_{e,\ cal}$ (mg g^{-1})	1.26	1.10	0.43
	k_2 (h^{-1})	1.19	2.81	0.46
	R^2	0.975	0.914	0.988
Weber–Morris	K_i (mg g^{-1} $h^{-0.5}$)	0.15	0.12	0.06
	B (mg g^{-1})	0.67	0.61	0.11
	R^2	0.965	0.949	0.999

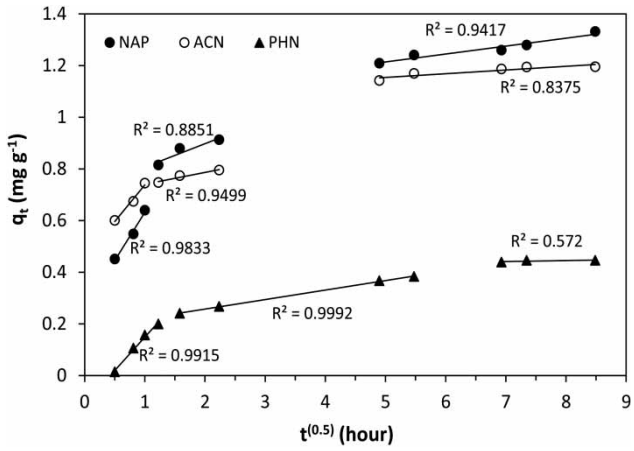

Figure 8 | Weber–Morris kinetic for NAP, ACN, and PHN adsorption onto NH_2-SBA-15 (conditions: pH 5, dosage 3 g L^{-1}, initial concentration of NAP, ACN, and PHN of 6, 6, and 4 mg L^{-1}, respectively).

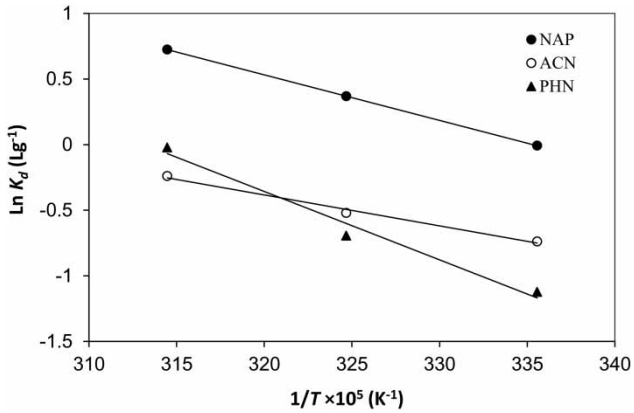

Figure 9 | Plots of ln k_d versus 1/T for NAP, ACN, and PHN adsorption onto NH_2-SBA-15 (conditions: adsorbent dose 3 g L^{-1}, pH 5, initial concentration of NAP, ACN, and PHN of 6, 6, and 4 mg L^{-1}, respectively).

Table 4 | Thermodynamic parameters of NAP, ACN, and PHN adsorption onto NH_2-SBA-15

			ΔG (kJ mol^{-1})			
PAHs	**ΔH (kJ mol^{-1})**	**ΔS ($J^{-1}mol^{-1}$ K^{-1})**	**Temperature (K)**			R^2
			293	313	333	
NAP	28.86	105.08	−2.45	−3.50	−4.55	0.999
ACN	19.62	78.89	−3.89	−4.68	−5.46	0.991
PHN	43.25	143.74	−0.42	−1.01	−2.45	0.978

Desorption

The stability and regeneration ability of the adsorbent is crucial for its practical application in wastewater treatment

(Ai *et al.* 2011). Hence, sequential adsorption/desorption cycles were carried out to evaluate practical utility of NH_2-SBA-15 organic–inorganic nanohybrid for PAH removal. The efficiencies of the adsorption–desorption cycle experiments are shown in Figure 10. The adsorption capacities decreased for each new cycle after desorption and this decreasing continued until the fifth cycle. The adsorption capacity of the NH_2-SBA-15 after five cycles indicated a loss in the adsorption capacity of 50.7% for NAP, 21.5% for ACN, and 29.7% for PHN compared to the initial cycle. The results showed that the adsorbent was stable without significant loss of the adsorption capacity up to three cycles. In this case, the desorption efficiencies were above 65%. Therefore, NH_2-SBA-15 could be successfully applied to successive cycles of adsorption–desorption.

Application of NH_2-SBA-15 for treating petroleum refinery wastewater

After optimizing the conditions using synthetic wastewater, the adsorption efficiency of NH_2-SBA-15 for removal of NAP, ACN, and PHN was studied using real petroleum refinery industry effluent, which was collected just at the egress of the A.P.I. treatment unit in the Tehran refinery plant, Iran. The standard method and reagents (USEPA 1999) were used for extracting and measuring target compounds in refinery wastewater samples (before and after each adsorption experiment set up), as well as for the calibration of GC (7890A, with HP5 column, film diameter 0.25 micrometer, diameter and column length 0.32 and 30, respectively, and temperature range +4 to 450 °C). Adsorption experiments were conducted in a batch system by adding 0.60 g adsorbent to 200 mL wastewater at pH 5 and temperature of 35 °C. The analysis of the target compounds showed that the efficiency of the applied NH_2-SBA-15 adsorbent was good for selected PAHs by removing 93% (1.67 mg g^{-1}), 97% (1.06 mg g^{-1}), and 85% (0.24 mg g^{-1}) of NAP, ACN, and PHN, respectively. By comparing the adsorption capacity of NH_2-SBA-15 for real and simulated wastewater it was revealed that the decreasing of adsorption capacity of NH_2-SBA-15 for real wastewater was insignificant. Therefore, NH_2-SBA-15 could be efficiently used for real wastewater treatment polluted by PAHs.

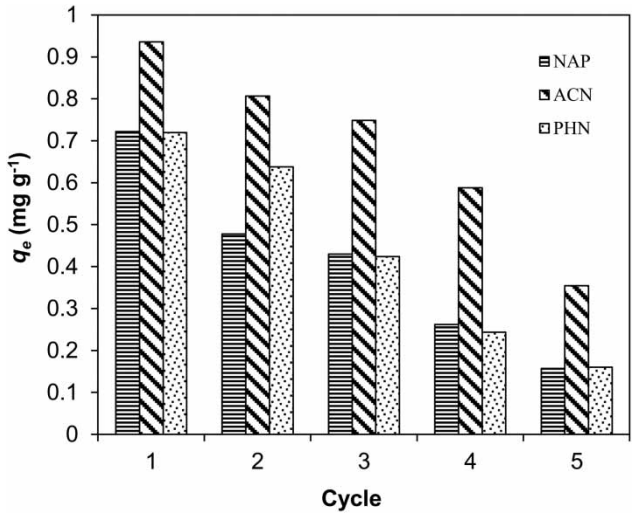

Figure 10 | Adsorption/desorption cycles of NAP, ACN, and PHN onto NH_2-SBA-15 (conditions: adsorbent dose 3 g L^{-1}, pH 5, and initial concentration of NAP, ACN, and PHN of 6, 6, and 4 mg L^{-1}, respectively).

CONCLUSION

The NH_2-SBA-15 organic–inorganic nanohybrid was prepared and used as adsorbent for NAP, CAN, and PHN removal. NH_2-SBA-15 exhibited good efficiency for PAH removal from aqueous solution in the order of NAP > ACN > PHN. Among isotherm models, the Langmuir model fitted the equilibrium data better than the Freundlich and Temkin isotherm, with a higher correlation coefficient. The maximum adsorption capacity NH_2-SBA-15 for NAP, ACN, and PHN based on the Langmuir model was 1.92, 1.41, and 0.76 mg g^{-1}, respectively. The kinetics of three adsorbates onto NH_2-SBA-15 revealed that adsorption kinetic could be satisfactorily described by pseudo-second-order model. The value of the Gibbs free energy of adsorption was found to be negative for all adsorbates, confirming the feasibility and spontaneity, as well as the endothermic nature of the adsorption process was conformed from positive values of enthalpy. The NAP, ACN, and PHN adsorption capacity was 0.73, 0.86, and 0.48 mg g^{-1}, respectively, for three regeneration cycles, showing an effective application for the treatment of wastewater containing these PAHs in successive cycles of adsorption–desorption. The results of adsorption experiments on real

petroleum refinery wastewater showed that NH_2-SBA-15 has a good efficiency in removal of the aforementioned compounds from liquid phase. In this case, adsorption capacity of 1.67, 1.06, and 0.24 mg g^{-1} of NAP, ACN, and PHN on NH_2-SBA-15 was achieved, respectively.

ACKNOWLEDGEMENTS

We would like to express our gratitude to the Iran National Science Foundation (INSF) for supporting this work. The authors are most grateful to Mr Hamed Bakhtiari in Tehran petroleum refinery for assisting.

REFERENCES

Aguado, J., Arsuaga, J. M., Arencibia, A., Lindo, M. & Gascón, V. 2009 Aqueous heavy metals removal by adsorption on amine-functionalized mesoporous silica. *J. Hazard. Mater.* **163** (1), 213–221.

Ai, L., Zhang, C. & Chen, Z. 2011 Removal of methylene blue from aqueous solution by a solvothermal-synthesized graphene/magnetite composite. *J. Hazard. Mater.* **192** (3), 1515–1524.

Anbia, M. & Moradi, S. E. 2009 Removal of naphthalene from petrochemical wastewater streams using carbon nanoporous adsorbent. *Appl. Surf. Sci.* **255** (9), 5041–5047.

Asouhidou, D. D., Triantafyllidis, K. S., Lazaridis, N. K. & Matis, K. A. 2009 Adsorption of remazol red 3bs from aqueous solutions using aptes- and cyclodextrin-modified hms-type mesoporous silicas. *Coll. Surf. A Physicochem. Eng. Asp.* **346** (1–3), 83–90.

Augulyte, L., Kliaugaite, D., Racys, V., Jankunaite, D., Zaliauskiene, A., Bergqvist, P.-A. & Andersson, P. L. 2009 Multivariate analysis of a biologically activated carbon (BAC) system and its efficiency for removing PAHs and aliphatic hydrocarbons from wastewater polluted with petroleum products. *J. Hazard. Mater.* **170** (1), 103–110.

Balan, C., Bilba, D. & Macoveanu, M. 2009 Studies on chromium (III) removal from aqueous solutions by sorption on sphagnum moss peat. *J. Serb. Chem. Soc.* **74** (8–9), 953–964.

Bereket, G., Arog, A. Z. & Özel, M. Z. 1997 Removal of Pb(II), Cd(II), Cu(II), and Zn(II) from aqueous solutions by adsorption on bentonite. *J. Coll. Interf. Sci.* **187** (2), 338–343.

Bui, T. X., Kang, S.-Y., Lee, S.-H. & Choi, H. 2011 Organically functionalized mesoporous SBA-15 as sorbents for removal of selected pharmaceuticals from water. *J. Hazard. Mater.* **193**, 156–163.

Cabal, B., Ania, C. O., Parra, J. B. & Pis, J. J. 2009 Kinetics of naphthalene adsorption on an activated carbon: Comparison between aqueous and organic media. *Chemosphere* **76** (4), 433–438.

Chang, C.-F., Chang, C.-Y., Chen, K.-H., Tsai, W.-T., Shie, J.-L. & Chen, Y.-H. 2004 Adsorption of naphthalene on zeolite from aqueous solution. *J. Coll. Interf. Sci.* **277** (1), 29–34.

Chen, Z., Zhou, L., Zhang, F., Yu, C. & Wei, Z. 2012 Multicarboxylic hyperbranched polyglycerol modified SBA-15 for the adsorption of cationic dyes and copper ions from aqueous media. *Appl. Surf. Sci.* **258** (13), 5291–5298.

Crisafully, R., Milhome, M. A., Cavalcante, R. M., Silveira, E. R., De Keukeleire, D. & Nascimento, R. F. 2008 Removal of some polycyclic aromatic hydrocarbons from petrochemical wastewater using low-cost adsorbents of natural origin. *Bioresour. Technol.* **99** (10), 4515–4519.

Gök, Ö., Özcan, A. S. & Özcan, A. 2008 Adsorption kinetics of naphthalene onto organo-sepiolite from aqueous solutions. *Desalination* **220** (1–3), 96–107.

Hall, S., Tang, R., Baeyens, J. & Dewil, R. 2009 Removing polycyclic aromatic hydrocarbons from water by adsorption on silica gel. *Polycycl. Aromat. Comp.* **29** (3), 160–183.

Hamoudi, S. & Belkacemi, K. 2013 Adsorption of nitrate and phosphate ions from aqueous solutions using organically-functionalized silica materials: Kinetic modeling. *Fuel* **110**, 107–113.

Hu, Q., Li, J. J., Hao, Z. P., Li, L. D. & Qiao, S. Z. 2009 Dynamic adsorption of volatile organic compounds on organofunctionalized SBA-15 materials. *Chem. Eng. J.* **149** (1–3), 281–288.

Jiang, J.-Q., Cooper, C. & Ouki, S. 2002 Comparison of modified montmorillonite adsorbents: Part I: Preparation, characterization and phenol adsorption. *Chemosphere* **47** (7), 711–716.

Khalili-Fard, V., Ghanemi, K., Nikpour, Y. & Fallah-Mehrjardi, M. 2012 Application of sulfur microparticles for solid-phase extraction of polycyclic aromatic hydrocarbons from sea water and wastewater samples. *Anal. Chim. Acta* **714**, 89–97.

Kosuge, K., Kubo, S., Kikukawa, N. & Takemori, M. 2007 Effect of pore structure in mesoporous silicas on voc dynamic adsorption/desorption performance. *Langmuir* **23** (6), 3095–3102.

Lemić, J., Tomašević-Čanovic, M., Adamović, M., Kovačević, D. & Milićević, S. 2007 Competitive adsorption of polycyclic aromatic hydrocarbons on organo-zeolites. *Micropor. Mesopor. Mater.* **105** (3), 317–323.

Lombardo, M. V., Videla, M., Calvo, A., Requejo, F. G. & Soler-Illia, G. J. A. A. 2012 Aminopropyl-modified mesoporous silica SBA-15 as recovery agents of cu(ii)-sulfate solutions: Adsorption efficiency, functional stability and reusability aspects. *J. Hazard. Mater.* **223–224**, 53–62.

Namasivayam, C. & Kavitha, D. 2002 Removal of congo red from water by adsorption onto activated carbon prepared from coir pith, an agricultural solid waste. *Dyes Pigments* **54** (1), 47–58.

Ofomaja, A. E. 2010 Intraparticle diffusion process for lead (II) biosorption onto mansonia wood sawdust. *Bioresour. Technol.* **101** (15), 5868–5876.

Oubagaranadin, J. U. K., Sathyamurthy, N. & Murthy, Z. 2007 Evaluation of fuller's earth for the adsorption of mercury from aqueous solutions: A comparative study with activated carbon. *J. Hazard. Mater.* **142** (1), 165–174.

Pérez-Gregorio, M. R., García-Falcón, M. S., Martínez-Carballo, E. & Simal-Gándara, J. 2010 Removal of polycyclic aromatic hydrocarbons from organic solvents by ashes wastes. *J. Hazard. Mater.* **178**, 273–281.

Prabhukumar, G. & Pagilla, K. 2010 *Polycyclic Aromatic Hydrocarbons in Urban Runoff–Sources, Sinks and Treatment: A Review*. Illinois Institute of Technology, Chicago.

Sasaki, T. & Tanaka, S. 2011 Adsorption behavior of some aromatic compounds on hydrophobic magnetite for magnetic separation. *J. Hazard. Mater.* **196**, 327–334.

Sevignon, M., Macaud, M., Favre-Réguillon, A., Schulz, J., Rocault, M., Faure, R., Vrinat, M. & Lemaire, M. 2005 Ultra-deep desulfurization of transportation fuels via charge-transfer complexes under ambient conditions. *Green Chem.* **7**, 413–420.

Shahbazi, A., Younesi, H. & Badiei, A. 2011 Functionalized SBA-15 mesoporous silica by melamine-based dendrimer amines for adsorptive characteristics of Pb(II), Cu(II) and Cd(II) heavy metal ions in batch and fixed bed column. *Chem. Eng. J.* **168** (2), 505–518.

Shahbazi, A., Younesi, H. & Badiei, A. 2012 Batch and fixed-bed column adsorption of Cu (II), Pb (II) and Cd (II) from aqueous solution onto functionalised sba-15 mesoporous silica. *Can. J. Chem. Eng.* **91** (4), 739–750.

Sherif, A., El-Safty, A. S. & Mohamed, I. 2012 Mesoporous aluminosilica monoliths for the adsorptive removal of small organic pollutants. *J. Hazard. Mater.* **201–202**, 23–32.

Srivastava, V. C., Swamy, M. M., Mall, I. D., Prasad, B. & Mishra, I. D. 2006 Adsorptive removal of phenol by bagasse fly ash and activated carbon: Equilibrium, kinetics and thermodynamics. *Coll. Surf. A Physicochem. Eng. Asp.* **272**, 89–104.

Tang, Y., Guo, H., Xiao, L., Yu, S., Gao, N. & Wang, Y. 2013 Synthesis of reduced graphene oxide/magnetite composites and investigation of their adsorption performance of fluoroquinolone antibiotics. *Coll. Surf. A Physicochem. Eng. Asp.* **424**, 74–80.

Temkin, M. I. & Pyzhev, V. 1940 Kinetics of ammonia synthesis on promoted iron catalysts. *Acta Physiochim.* **12**, 217–222.

USEPA 1999 *Standard Methods for the Examination of Water and Wastewater*, 20th edn. Method 6440 b. Liquid–liquid extraction chromatographic method, Part 4000. United States Environmental Protection Agency, Washington, DC.

Vidal, C. B., Barros, A. L., Moura, C. P., De Lima, A. C. A., Dias, F. S., Vasconcellos, L. C. G., Fechine, P. B. A. & Nascimento, R. F. 2011 Adsorption of polycyclic aromatic hydrocarbons from aqueous solutions by modified periodic mesoporous organosilica. *J. Coll. Interf. Sci.* **357** (2), 466–473.

Vijayakumar, G., Tamilarasan, R. & Dharmendirakumar, M. 2012 Adsorption, kinetic, equilibrium and thermodynamic studies on the removal of basic dye rhodamine-b from aqueous solution by the use of natural adsorbent perlite. *J. Mater. Environ. Sci.* **3** (1), 157–170.

Wei, X., Husson, S. M., Mello, M. & Chinn, D. 2008 Removal of branched dibenzothiophenes from hydrocarbon mixtures via charge transfer complexes with a TAPA-functionalized adsorbent. *Eng. Chem. Res.* **47**, 4448–4454.

Wu, Z. & Zhu, L. 2012 Removal of polycyclic aromatic hydrocarbons and phenols from coking wastewater by simultaneously synthesized organobentonite in a one-step process. *J. Environ. Sci.* **24** (2), 248–253.

Yang, X., Li, J., Wen, T., Ren, X., Huang, Y. & Wang, X. 2013 Adsorption of naphthalene and its derivatives on magnetic graphene composites and the mechanism investigation. *Coll. Surf. A* **422**, 118–125.

Zhao, D., Feng, J., Huo, Q., Melosh, N., Fredrickson, G. H., Chmelka, B. F. & Stucky, G. D. 1998a Triblock copolymer syntheses of mesoporous silica with periodic 50 to 300 angstrom pores. *Science* **279** (5350), 548–552.

Zhao, D., Huo, Q., Feng, J., Chmelka, B. F. & Stucky, G. D. 1998b Nonionic triblock and star diblock copolymer and oligomeric surfactant syntheses of highly ordered, hydrothermally stable, mesoporous silica structures. *J. Am. Chem. Soc.* **120** (24), 6024–6036.

Zhao, G., Li, J. & Wang, X. 2011 Kinetic and thermodynamic study of 1-naphthol adsorption from aqueous solution to sulfonated graphene nanosheets. *Chem. Eng. J.* **173** (1), 185–190.

First received 16 February 2014; accepted in revised form 29 July 2014. Available online 18 August 2014